



HAL
open science

Modeling particle deposition in the primary circuit of pressurized water reactors for the OSCAR code

Chloé Cherpin, Frédéric Dacquait

► **To cite this version:**

Chloé Cherpin, Frédéric Dacquait. Modeling particle deposition in the primary circuit of pressurized water reactors for the OSCAR code. *Annals of Nuclear Energy*, 2024, 199, pp.110364. 10.1016/j.anucene.2024.110364 . cea-04574491

HAL Id: cea-04574491

<https://cea.hal.science/cea-04574491>

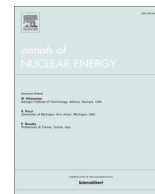
Submitted on 14 May 2024

HAL is a multi-disciplinary open access archive for the deposit and dissemination of scientific research documents, whether they are published or not. The documents may come from teaching and research institutions in France or abroad, or from public or private research centers.

L'archive ouverte pluridisciplinaire **HAL**, est destinée au dépôt et à la diffusion de documents scientifiques de niveau recherche, publiés ou non, émanant des établissements d'enseignement et de recherche français ou étrangers, des laboratoires publics ou privés.



Distributed under a Creative Commons Attribution - NonCommercial - NoDerivatives 4.0 International License



Modeling particle deposition in the primary circuit of pressurized water reactors for the OSCAR code

Chloé Cherpin^{*}, Frédéric Dacquait

CEA, DES, IRESNE, DTN, Cadarache F-13108, Saint-Paul-Lez-Durance, France

ARTICLE INFO

Keywords:

Activity transfer
Primary circuit
PWR
OSCAR code
Deposition
Corrosion products

ABSTRACT

Particulate corrosion products are generated in the primary system of pressurized water reactors (PWRs) by volume precipitation and by erosion of oxides formed on metal surfaces through their uniform corrosion. The activation of corrosion products, mainly ^{58}Co and ^{60}Co (respectively coming from the activation of ^{58}Ni and ^{59}Co) leads to radiation field growth around the primary system, directly impacting system integrity and the radioprotection of nuclear workers. In order to understand and mitigate contamination by activated corrosion products, contamination predictions can be performed using the OSCAR code, which relies on the development of models to describe the numerous and complex interactions at stake. Particulate corrosion products account for a significant portion of corrosion products, as such the deposition/erosion mechanisms have their importance for the overall computation of surface or volume contamination. The aim of this article is to present an updated and inclusive deposition model for particulate corrosion products by taking into account surface interactions. The impact of the new deposition model on contamination predictions is then evaluated and has enabled to reproduce, for the first time using the OSCAR code, the preferential contamination in ^{58}Co in the cold side of the circuit, measured by gamma spectrometry with the EMECC device on commercially PWRs.

1. Introduction

In pressurized water reactors (PWRs), uniform corrosion of metals (mainly stainless steels and nickel based alloys) in contact with the primary coolant (light water conditioned with a coordinated boron/lithium chemistry, between 280 and 320 °C) leads to the formation of a double layer oxide at the interface metal/coolant and to the release of ionic species in the solution (Carrette, 2002; Gardey, 1998; Lister, 2012; Marchetti-Sillans, 2007; Millett, 1999). The erosion of oxides as well as local solubility differences result in the presence of particles in the coolant, which are commonly referred to as particulate corrosion products (CPs). Should CPs deposit in a zone under neutron flux, they might be activated and form activated corrosion products (ACPs), inducing volume contamination (if they remain suspended or dissolved) or surface contamination (if they deposit or precipitate on an out-of-flux surface).

The prediction of activity transfer by ACPs in the primary system of PWRs is of the utmost importance as ACPs are responsible for 85 % of the collective dose received by workers during maintenance operations (Anthoni and Ridoux, 1996). In addition to having detrimental

consequences for the radioprotection of nuclear operators, ACPs are also unfavourable for system integrity as their deposition on fuel rods surfaces causes Crud induced Power Shift (CIPS) (Deshon et al., 2011), forcing plants to reduce power (Lister, 2012), sometimes to as low as 70 %, or even causing higher corrosion rates on fuel cladding through Crud Induced Localized Corrosion (CILC). Among the main ACPs found in the primary system, ^{58}Co (activation of ^{58}Ni) and ^{60}Co (activation of ^{59}Co) are the most troublesome from a radioprotection standpoint as they account for over 90 % of the average dose emitted by ACPs around the primary system (Dacquait et al., 2004).

Corrosion products are transported in the primary system either as ions (coming from the release term due to the corrosion of the base metal or from the dissolution of oxides) or as particles (coming from the erosion of oxides and from volume precipitation). General trends concerning the proportion of corrosion products under particulate form in the primary system are difficult to establish as each plant has its specificities. Nonetheless, a filtration campaign performed during operation on a 1300 MWe PWR NPPs (Dacquait et al., 2008) has shown that respectively 85 % and 70 % of ^{58}Co and ^{60}Co volume activity is carried as particles with a size above 0.45 μm . This justifies that mechanisms

^{*} Corresponding author.

E-mail addresses: chloe.cherpin@cea.fr (C. Cherpin), frederic.dacquait@cea.fr (F. Dacquait).

describing particulate transfer are essential to model and predict activity transfer and contamination around the reactor coolant system (RCS) (Cherpin, 2022). In particular, particle deposition is a key mechanism as it is directly linked to the source term in ACPs, as ACPs are generated by CPs deposition on in-flux regions, and to surface contamination, generated by the deposition of ACPs on out-of-flux surfaces.

The deposition of particles onto a surface, under isothermal conditions, is usually described as the succession of two independent steps in series (Epstein, 1988a): a transport step and an attachment step, each described by their coefficient K_t and K_a respectively so that the deposition coefficient K_D ($\text{m}\cdot\text{s}^{-1}$) is:

$$\frac{1}{K_D} = \frac{1}{K_T} + \frac{1}{K_A} \quad (1)$$

The transport step corresponds to the transport of the particle from the bulk of the fluid to the wall (surface) considered and the attachment step corresponds to the attachment of the particles on this wall. The determination of the deposition coefficient therefore requires the knowledge of the transport and of the attachment coefficient.

As particle size ranges from below $1 \mu\text{m}$ to several micrometers (Bridle, 1989; Dacquait et al., 2002; Frattini, 1999; Strasser, 1996; Wen, 1998), it is essential to take into account characteristics pertaining to both inertial and colloidal particles when modelling their transport and attachment (Rodliffe, 1985). Therefore, when modeling deposition, surface interactions (predominant for colloids deposition) as well as volume interactions (predominant for inertial particles) have to be considered.

This paper presents the OSCAR tool, for which an inclusive deposition model is developed. It then focuses on the updated deposition model and presents simulation results obtained with the new deposition model, with which a preferential contamination in ^{58}Co in the cold part of the circuit was reproduced for the first time ever using the OSCAR code, confirming measurements performed on operating PWRs.

2. Theory

2.1. The OSCAR code

OSCAR stands for Outil de Simulation de la Contamination en Réacteur in French, translated as tOol for Simulating Contamination in Reactors. This code originates from the merging of the calculation codes PACTOLE for ACPs (Beslu, 1990; Beslu et al., 1978) and PROFIP for fission products. It is developed by the CEA (French Alternative Energies and Atomic Energy Commission) in collaboration with EDF and

Framatome. This tool is able to simulate activity transfer in nuclear reactor systems by computing the evolution of the mass of corrosion products, fission products and actinides in the primary circuit with time. The OSCAR code works for a wide range of conditions including power operations and shutdowns, thus covering a large range of temperatures (from $20 \text{ }^\circ\text{C}$ to $350 \text{ }^\circ\text{C}$) and conditions (reducing/oxidizing and acid/alkaline), which is a significant improvement compared to other codes (other codes aiming at performing similar calculations were reviewed by Rafique et al. (2010)). Furthermore, the OSCAR simulation tool is unique as its calibration and validation are performed using an exclusive database of surface contamination levels measured on operating PWRs during shutdown. These measurement campaigns employing a gamma spectrometry method are referred to as EMECC campaigns and have been performed for more than 50 years. The OSCAR code was originally developed for the primary system of PWRs but is also applied to fusion reactors (OSCAR-Fusion) (Dacquait et al., 2017) and sodium-cooled fast neutron reactors (OSCAR-Na) (Génin and Brissonneau, 2017).

The OSCAR modelling starts by nodalizing the circuit studied, here the primary system and its purification system (CVCS), into control volumes as shown in Fig. 1. Each control volume is defined by its geometry and various characteristics (thermohydraulics, neutronic...) and by its base metal.

Within each control volume, various media are considered including:

- the base metal which is the alloy (stainless steel, nickel based alloys...) and undergoes generalized corrosion.
- the inner oxide which formation results from generalized corrosion. The inner oxide is a non-porous chromium rich layer and adopts the structure of a spinel chromite (e.g., $\text{Ni}_x\text{Co}_y\text{Fe}_z\text{Cr}_{3-x-y-z}\text{O}_4$, particularly stable, with $y \ll x + z$) (Lister, 2012)
- the outer oxide and deposit layer is formed by crystals with an inverse spinel ferrite structure (often a non-stoichiometric nickel ferrite $\text{Ni}_x\text{Co}_y\text{Fe}_z\text{Fe}_{3-x-y-z}\text{O}_4$ with $x \approx 0.6$ and $y \ll x + z$) (Carrette, 2002; Gardey, 1998; Marchetti-Sillans, 2007) coming from the precipitation of ions and the deposition of particles. It is assumed that the outer oxide/deposit is porous.
- Ions are transported by advection around the primary circuit and come from the release term due to the generalized corrosion of the base metal and from the dissolution of the inner oxide or outer oxide/deposit.
- Particles, which are transported by advection, come from the precipitation of ions or from the erosion of the outer oxide/deposit.

The chemical elements constitute of the alloys encountered in the

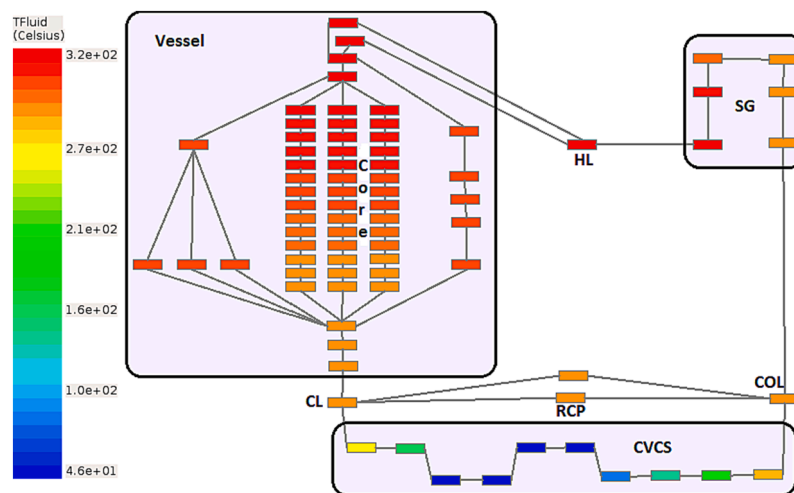


Fig. 1. Control volumes of the primary system of a PWR (CL: Cold Leg, HL: Hot Leg, SG: Steam Generator, COL: Crossover Leg, CVCS: Chemistry volume and control Volume, RCP: Reactor Coolant Pump).

primary circuit are considered including Fe, Ni, Co, Cr, Mn and Zr. These elements can become activated under neutron flux.

A steady mass balance equation is solved for each isotope, in each medium, in each control volume:

$$\frac{\partial m_{i,j}}{\partial t} = \sum_{source} J_m - \sum_{sink} J_m + m_{in} - m_{out} \quad (2)$$

Where m_i is the mass of the isotope i in a media j , J_m the mass flux between two media or two isotopes and $m_{in} - m_{out}$ the advection term.

Fig. 2 shows the different mechanisms involved in the transfers between the various media considered in the OSCAR code (Dacquait et al., 2023, p. 60). The OSCAR code is a multiphysic tool as it considers the interactions between neutronics (activation, decay), hydrodynamics (advection, deposition,..), chemistry (precipitation/dissolution...) and electrochemistry (i.e. corrosion) aspects.

Among these mechanisms, the deposition of particles is at the heart of this paper.

2.2. Deposition model

2.2.1. Beal model for the deposition of particles

The previous deposition model implemented in the OSCAR code (up to version 1.4.a included) relies on the Beal modelling of particles deposition (Beal, 1978, 1970). In this model which unifies the description of Brownian particles (Lin et al., 1953) and large particles (Friedlander and Johnstone, 1957) developed in the seventies, particles are transported from the bulk to a distance S from the surface, called stopping distance, notion borrowed to Friendlander and Johnstone (Friedlander and Johnstone, 1957), by turbulent diffusion. After this stopping distance, particles get to the surface due to their inertia only. The stopping distance of a particle is expressed as follows (Beal, 1970):

$$S = \frac{\rho_p d_p^2 V_p(y)}{18\mu} + \frac{d_p}{2} \quad (3)$$

Where ρ_p is the density of the particle, d_p the diameter of the particle, $V_p(y)$ the radial velocity of the particle at a distance y from the surface, μ the dynamic viscosity of the fluid.

The velocity of the particle $V_p(y)$ is obtained by solving the following momentum balance:

$$m_p V_p(y) \frac{dV_p(y)}{dy} = -3\pi d_p \mu (v' - V_p(y)) \quad (4)$$

Where m_p is the mass of the particle, d_p the diameter of the particle, μ the dynamic viscosity of the fluid and v' the fluctuations of the radial velocity of the particles.

The velocity of the particle $V_p(y)$ consists of two components in the Beal model: a component due to the motion of the fluid normal to the surface, $V_f(y)$ (Laufer, 1954), and a component due to the Brownian motion (in the direction of the surface), V_b , as follows:

$$V_b = \sqrt{\frac{k_b T}{2\pi m_p}} \quad (5)$$

Where k_b is Boltzmann constant, T the temperature of the fluid and m_p the mass of the particle.

The component due to the motion of the fluid normal to the surface $V_f(y)$ is more used under its dimensionless form v_f^+ :

$$\begin{cases} v_f^+ = 0.05y^+ & \text{if } 0 \leq y^+ \leq 10 \\ v_f^+ = 0.5 + 0.0125(y^+ - 10) & \text{if } 10 \leq y^+ \leq 30 \end{cases} \quad (6)$$

Where $y^+ = \frac{yU\sqrt{f}}{\nu}$ (U the average fluid velocity, f Fanning friction factor, ν the kinematic viscosity), and $v_f^+ = \frac{v_f}{U\sqrt{f}}$.

The attachment of the particle onto a surface is quantified through the notion of sticking probability p_{beal} . This sticking probability is linked to the stopping distance using experiments described in Beal's study (Beal, 1978). This first expression for the sticking probability was derived from experiments conducted by Sehmel (1971), in which the deposition of particles ranging in size from 8 to 10 μm in air with a velocity ranging from 9 to 30 m/s was studied, and is as follows:

$$\begin{cases} p_{beal} = 1 & \text{if } S^+ \leq 4.5 \\ p_{beal} = \left(\frac{4.5}{S^+}\right)^4 & \text{if } S^+ > 4.5 \end{cases} \quad (7)$$

This second expression for p_{beal} was produced using experiments performed by Watkinson (Watkinson, 1968), where the deposition of 15 μm sand particles in water at 20 °C, and gave the following sticking probability expression:

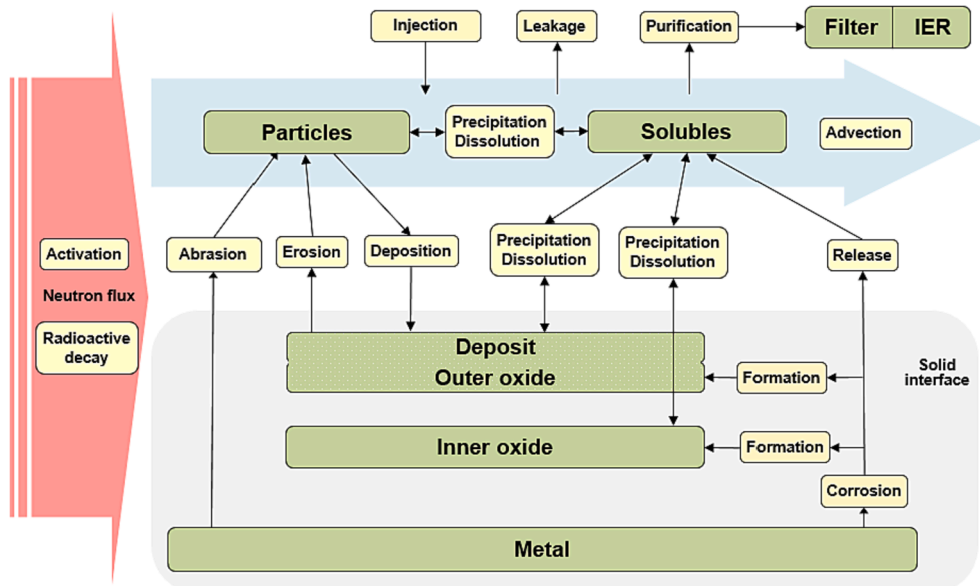


Fig. 2. Different mechanisms taken into account in the OSCAR code in a given control volume or region.

$$\begin{cases} p_{beal} = 1 & \text{if } S^+ \leq 2.4 \\ p_{beal} = \left(\frac{2.4}{S^+}\right)^4 & \text{if } S^+ > 2.4 \end{cases} \quad (8)$$

Where S^+ is the dimensionless stopping distance:

$$S^+ = \frac{S\bar{U}\sqrt{f/2}}{\nu} \quad (9)$$

Where \bar{U} is the average fluid velocity, f the Fanning friction factor and ν the kinematic viscosity.

Considering the conditions of the hot leg (HL) and cold side of the Steam Generator (SG) in the primary circuit during operations ($T_{HL} \approx 330$ °C and $T_{SG,cold} \approx 290$ °C), the Beal sticking probability p_{beal} (using Watkinson experiments as they were performed in water) can be computed as a function of the particle radius (see Fig. 3). In the hot leg, if the particle radius is superior to 0.5 μm , its deposition probability is null, whereas in the cold side of the SG this limit radius is estimated around 1 μm .

As seen previously, the expression of the sticking probability is highly dependent on the experiment, which lacks representativeness for primary circuit conditions. Also, surface interactions are not accounted for in the Beal modelling of particle deposition. Therefore a new deposition model was developed in order to take into account the behavioural specificities of both inertial and colloidal particles.

2.2.2. A new expression for the deposition velocity

The deposition rate $J_{deposition}^{i,reg}$ for an isotope i under particulate form in a region reg is calculated as follows:

$$J_{deposition}^{i,reg} = S_m \alpha_{deposition} V_{deposition} F_{enrich} C_i \quad (10)$$

Where S_m is the wet surface between the fluid and the wall, $\alpha_{deposition}$ is a calibration coefficient for the deposition rate (equal to 0.1 in OSCAR v1.4.a), $V_{deposition}$ is the deposition velocity, F_{enrich} an enrichment factor in case of boiling and C_i the particulate concentration of isotope i .

Previously, the expression of the deposition velocity was dependant on the flow regime. A unified expression has been developed. Deposition is modelled as the succession of the transport step and the attachment step (Epstein, 1988b). During the transport step, sedimentation, which plays a significant role for large particles in a horizontal pipe, as well as mass transfer due to the flow (whether it is laminar or turbulent) and thermophoresis (caused by a thermal gradient in the fluid and resulting in a driving force) are considered. The resistance to transport $R_{transport}$ can then be written as follows:

$$R_{transport} = \frac{1}{h' + V_{sed}} \quad (11)$$

Where h' is the mass transfer coefficient taking into account thermophoresis, and V_{sed} the sedimentation velocity.

The mass transfer coefficient h' taking into account thermophoresis is:

$$h' = \frac{V_{thermo}}{e^{\frac{V_{thermo}}{h}} - 1} \quad (12)$$

Where V_{thermo} is the thermophoresis velocity (Ponting, 1983) and h the mass transfer coefficient, which expression was established in Beal (Beal, 1970) according to the regime of the flow.

For the attachment step, the resistance $R_{transport}$ can be written as follows:

$$R_{transport} = \frac{1}{pV_{rad}} \quad (13)$$

Where p is the attachment probability and V_{rad} the radial velocity of the particle when it touches the wall.

As the transport step and the attachment step are in series, the total resistance to deposition $1/V_{deposition}$ is:

$$\frac{1}{V_{deposition}} = \frac{1}{h' + V_{sed}} + \frac{1}{pV_{rad}} \quad (14)$$

2.2.3. New expression for the attachment probability

In order to replace the sticking probability established by Beal, which depends on the stopping distance, a new expression, which can represent both inertial and colloidal effects, is proposed. As the attachment of particles is intrinsically related to surface forces, the sticking probability, called in the rest of the paper, attachment probability, has to take into account these effects. When a particle approaches a surface, several interactions will determine if the particle can attach to the surface: mainly the London Van der Waals interaction, the electrostatic static interaction and the Born interaction, making up for the DLVO theory (Derjaguin and Landau, 1941; Verwey and Overbeek, 1948). In certain conditions, if the particle and the surface have surface charges of the same sign, a potential barrier will appear between the two. According to Urrutia et al. (1983), a particle can deposit onto a surface if its kinetic energy is sufficient to overcome the potential barrier. An energy ratio P_s can thus be defined as the ratio of the kinetic energy of the particle arriving onto the surface to the potential barrier K to overcome:

$$P_s = \frac{\frac{1}{2}m_p v_p}{K} \quad (15)$$

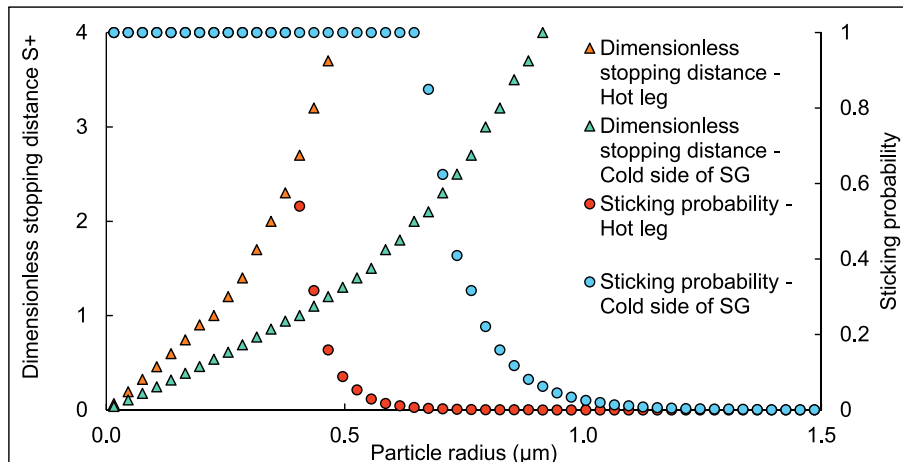


Fig. 3. Variation of the Beal sticking probability established using Watkinson experiment with the particle radius in the conditions of the hot leg of a 900 MWe PWR.

According to Rudolph (2016), an attachment probability p taking into account surface effects can then be established as follows:

$$\begin{cases} p = 0 & \text{if } P_s < 1 \\ p = \frac{1}{1 + Ae^{BP_s}} & \text{if } P_s \geq 1 \end{cases} \quad (16)$$

Where A and B are two parameters to be calibrated. Qualitatively, such an attachment probability profile (shown in Fig. 4) reflects that if the energy ratio P_s is inferior to 1, the kinetic energy of the particle is not sufficient to overcome the potential barrier and there is no deposition. For an energy ratio P_s equal to 1, the attachment probability is maximum. As the velocity of the particle increases, hydrodynamic effects become increasingly important, thus decreasing the probability of attachment, as re-entrainment is more likely to happen (see Fig. 5).

2.2.4. Evaluation of the potential barrier value

The potential barrier existence and value is evaluated using the DLVO (Derjaguin, Landau, Vervy and Overbeek) (Derjaguin, 1993) theory. The total interaction potential ϕ_T arising from the approach of a particle can be expressed as the sum of the attractive interactions ϕ_A and the repulsive interactions ϕ_R :

$$\phi_T = \phi_A + \phi_R \quad (17)$$

In the classic DLVO theory, the attractive forces consist of the Van der Waals forces (equation (16)) and the electrical double layer force (equation (17)) (if the particle and the surface have surface charges of opposite sign); likewise, the repulsive forces consist of the electrical double layer force (equation (17)) (if the particle and the surface have surface charges of same sign) and the Born repulsive force (equation (18)) (due to the repulsion between the atomic orbitals of the particle and of the surface).

$$\phi_{vdw}(h) = -\frac{Ar_p}{6h} \left(\frac{1}{1 + 14\frac{h}{\lambda}} \right) \quad (18)$$

Where A is Hamaker constant, r_p the particle radius, h the distance separating the particle from the surface and λ the characteristic length of retardation effect.

$$\phi_{EDL}(h) = \pi\epsilon_0\epsilon_r r_p \left[2\psi_p\psi_s \ln\left(\frac{1 + e^{-\kappa h}}{1 - e^{-\kappa h}}\right) + (\psi_p^2 + \psi_s^2) \ln(1 - e^{-2\kappa h}) \right] \quad (19)$$

Where ϵ_0 is the permittivity of free space, ϵ_r the relative permittivity of the solution, r_p the particle radius, ψ_s the surface potential of the wall (surface), ψ_p the surface potential of the particle, κ the inverse Debye length and h the distance separation the particle from the surface.

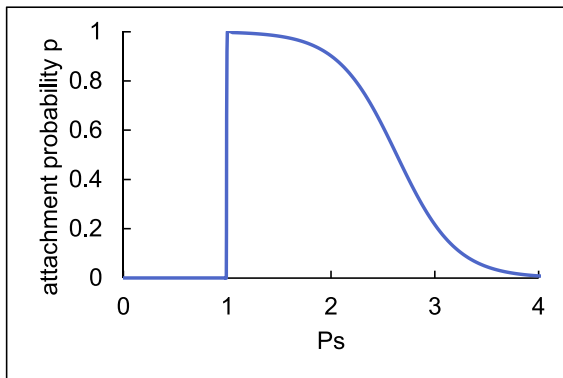


Fig. 4. Attachment probability established by Rudolph (Rudolph, 2016) with $A = 10^{-4}$ and $B = 3.5$.

$$\phi_{Born}(h) = \frac{A\sigma_{born}^6}{7560} \left[\frac{8r_p + h}{(2r_p + h)^7} + \frac{6r_p - h}{h^7} \right] \quad (20)$$

Where σ_{born} is Born collision parameter.

2.2.5. Zeta potential values

As expressed in equation (17), the electrical double layer interaction requires the knowledge of the surface potential of the particle and the surface. The surface potential ψ can be computed from the zeta potential ζ through equation (19) (Van Oss et al., 1990):

$$\psi = \zeta \left(1 + \frac{z}{r_p} \right) e^{\kappa z} \quad (21)$$

Where z equals 5 \AA , r_p is the particle radius and κ the inverse Debye length. Equation (19) remains valid assuming that the particle size is much larger than the thickness of the double layer (approximated by the Debye length) and for small zeta potential values (Van Oss et al., 1990).

The knowledge of the zeta potential values of the corrosion products generated in the primary system is required to compute the electrical double layer interaction and in turn the value of the potential barrier to overcome for deposition. In a previous study (Cherpin et al., 2021, 2022a, 2022b), the zeta potential of magnetite and nickel ferrite was determined between $20 \text{ }^\circ\text{C}$ and $240 \text{ }^\circ\text{C}$ using a custom built test section implementing the streaming potential method. For twelve different boron/lithium coordinations, the zeta potential of these two commonly encountered corrosion products was determined.

As shown in a previous study, the temperature and the pH have a strong influence on the zeta potential value (Cherpin et al., 2022b), therefore the expression for the zeta potential value was chosen to be a second degree law with pH and temperature, as follows:

$$\zeta = p_{00} + p_{10}T + p_{01}pH + p_{20}T^2 + p_{11}TpH + p_{02}pH^2 \quad (22)$$

The parameters $p_{00}, p_{10}, p_{01}, p_{20}, p_{02}$ and p_{11} where optimized to obtain the best fit between the experimental data and the zeta potential values obtained with equation (22). Here is a graphical representation of the interpolation for the magnetite particles:

This interpolation gave a coefficient of determination for magnetite and nickel ferrite respectively equal to 0.78 and 0.57. It is assumed that this interpolation can be extrapolated for conditions representative of the primary circuit (between $280 \text{ }^\circ\text{C}$ and $340 \text{ }^\circ\text{C}$, for continuous boron/lithium chemistries), as no other data is available.

3. Results and discussion

3.1. Validation of the deposition model

3.1.1. CIRENE experiments

The previously described deposition model was implemented in the calculation kernel of the OSCAR code. It was then calibrated using experiments performed on the CIRENE loop, operated in the CEA. The CIRENE loop is a test loop that enables the reproduction of primary circuit conditions for studying particle deposition kinetics, among other aspects (Girard and Dacquait, 2012). During typical CIRENE experiments, particles of known composition and size distribution are injected in the loop through a powder injection device. The particle concentration is then followed in the loop using an in-line particle counting system as shown in Fig. 6, giving access to the deposition kinetics of particles. The loop consists of two main sections: a core section in Zircaloy 4 (representative of fuel rods of a PWR) and a steam generator (SG) section in Alloy 690.

By running simulations using a dataset representative of the CIRENE loop and of the chosen experiment, the attachment probability profile proposed by Rudolph (equation (16)) has been calibrated.

Two CIRENE experiments are used in this paper (Girard and Mombellet, 2011). Experiment A consists in an injection of 40 mg of

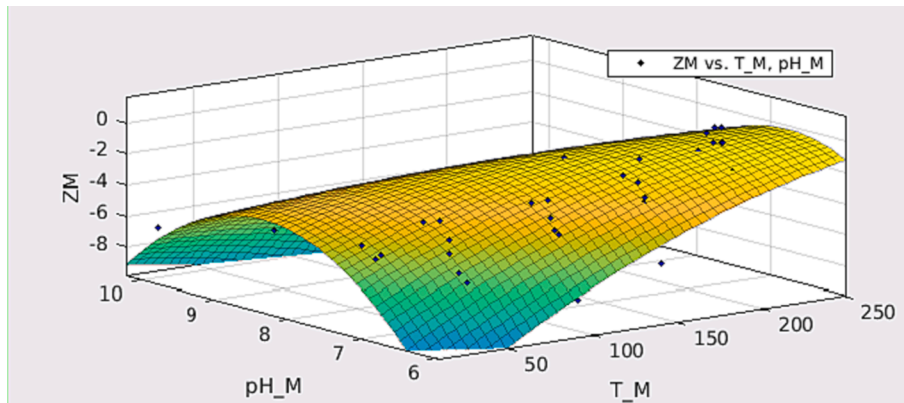


Fig. 5. Polynomial interpolation of the zeta potential of magnetite (ZM) as a function of the temperature (T_M in $^{\circ}\text{C}$) and pH (pHM).

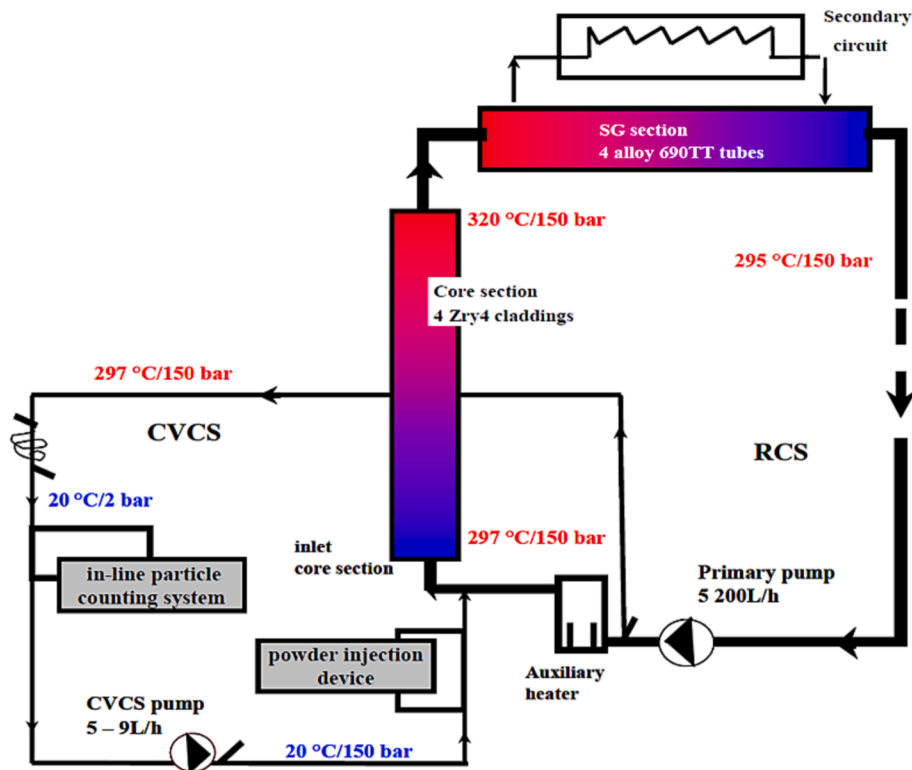


Fig. 6. CIRENE loop outlines required for powder injection and particles counting (Girard and Dacquait, 2012).

magnetite (Fe_3O_4) powder during 4 min 20 s in the CIRENE primary loop (RCS) conditioned with 100 ppm of boron and 0.6 ppm of lithium, giving a pH of 7.35 at 300 $^{\circ}\text{C}$. The magnetite powder was purchased at Sigma Aldrich (purity 98 %, particle size $\leq 1 \mu\text{m}$). The experimental particle concentration was measured and is shown in Fig. 6.

After 915 s from injection, the particle concentration reaches a maximum. After this peak, the decrease in particle concentration is due to particles deposition, as their dissolution is negligible in the CIRENE loop conditions (dissolution kinetic negligible on the time scale of the experiment compared to deposition kinetic, confirmed by particle size distribution measurements performed before and after the experiments). After a certain time after injection, the number of particles in the loop remains non-negligible (around 1000 particles per mL) due to the erosion of surfaces.

The second experiment used in this paper, Experiment B, was also conducted in 2010 and consisted in the injection of 190 mg of nickel particles (purchased in Sigma-Aldrich with a particle size inferior to 3

μm , purity 99.7 %) during 4 min 20 s. Fig. 7 shows the evolution of the particle concentration measured in the CIRENE loop after injection.

3.1.2. Validation of the deposition model

Fig. 8 shows, for Experiment A, the particle concentration obtained using the optimized Rudolph attachment probability profile plotted with the prediction obtained using the previous version of the code (OSCAR v1.4.a) which did not take into account surface interactions. Also, as mentioned in equation (8), the version 1.4.a of the OSCAR code required the use of a calibration coefficient equal to 0.1 to compute the deposition rate of particles, which is not the case for the new deposition model, for which no corrective coefficient is applied.

For experiment A, the use of the optimized Rudolph function gives a better result than with the previous sticking probability from Beal.

Fig. 9 shows the prediction obtained with the new calibrated deposition model for Experiment B. The prediction is acceptable.

The optimized Rudolph function gives a better prediction for

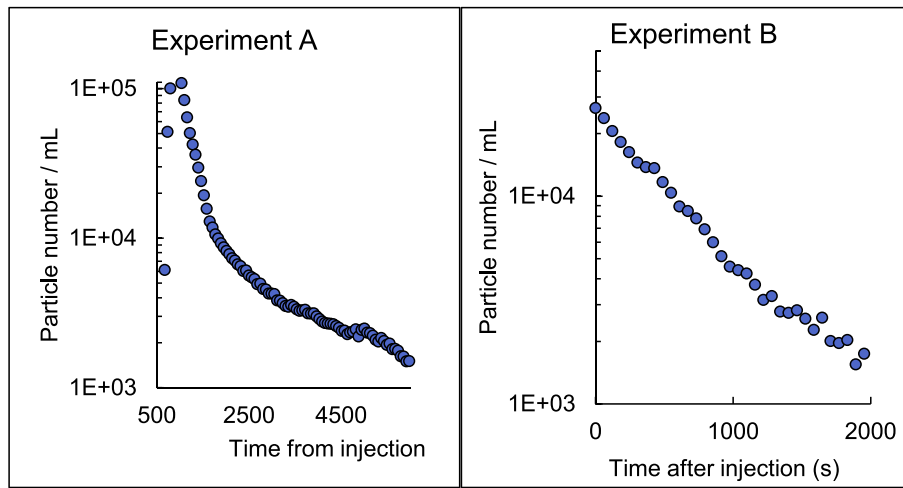


Fig. 7. Experimental particle concentration measured in the CIRENE loop after injection corresponding to Experiment A and Experiment B.

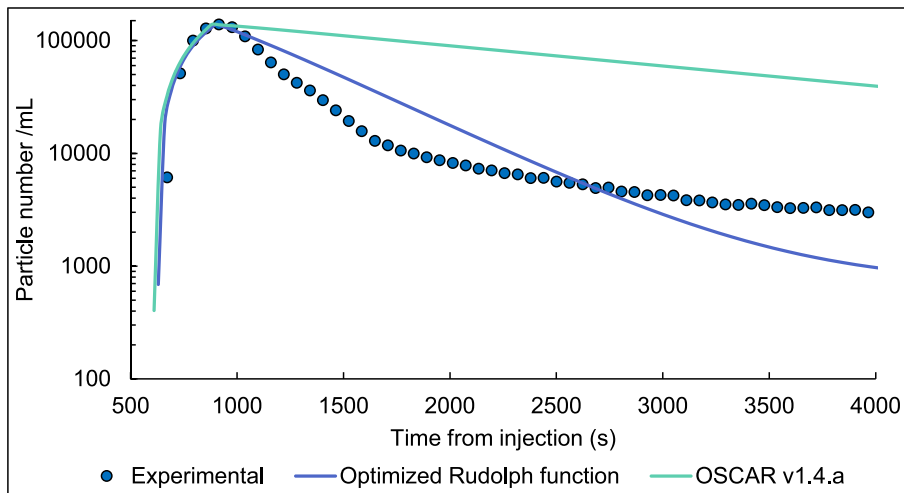


Fig. 8. Evolution of the particle concentration simulated using the optimized attachment profile and the previous version of the OSCAR code (v1.4.a) (Experiment A).

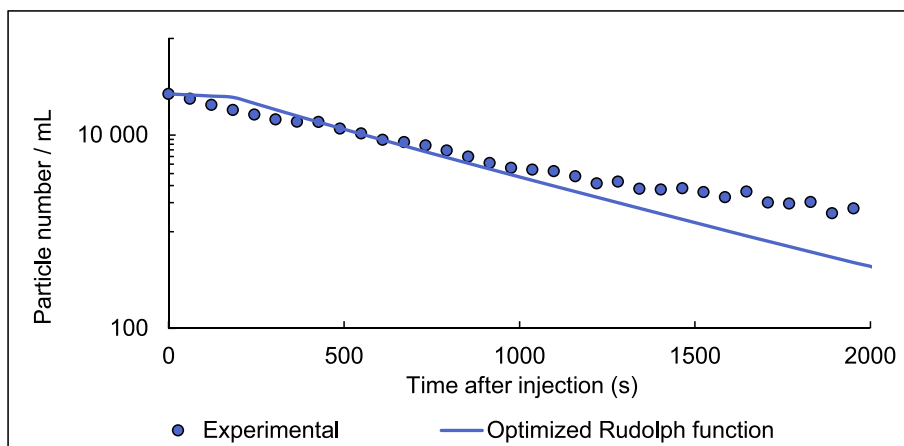


Fig. 9. Evolution of the particle concentration simulated using the optimized attachment profile (Experiment B).

Experiment B than for Experiment A, mostly due to the calibration of parameters A and B (equation (16)), which values might depend on the nature of the particles injected. This idea will be explored in future work.

3.2. Simulation results

Using the previously described deposition model, the OSCAR code is

used to simulate the contamination levels in the primary circuit of an operating 1300 MWe PWR, referred to as Reactor A in the rest of the paper, with a particular background. Indeed, this reactor underwent a Steam Generator Replacement (SGR) and one operating cycle later (cycle SGR + 1), the EMECC device was used to measure via gamma spectrometry the surface contamination levels, particularly ^{58}Co . These measurements showcased a preferential contamination of the crossover leg in ^{58}Co compared to other regions such as the hot leg as shown in Fig. 10. Such a difference in terms of surface contamination between the crossover leg and the hot leg had never been measured before. Indeed Fig. 11 shows the ^{58}Co surface contamination levels between the hot leg and the crossover leg for 8 reactors including Reactor A in red. Usually, the crossover leg is between 1.4 and 2 times more contaminated than the hot leg, however for Reactor A, it is 10 times more contaminated.

When using the previous version of the OSCAR code in which surface interactions and therefore colloids behavioural specificities are ignored, the surface contamination levels cannot be reproduced as shown in Fig. 12.

The EMECC measurements have shown that the surface contamination regarding ^{60}Co are similar between the hot leg and the crossover leg for Reactor A at cycle SGR + 1, whereas a preferential contamination in ^{58}Co was measured in the crossover leg. This different behaviour is likely to be explained by a different transfer mechanism between ^{58}Co and ^{60}Co . Indeed, ^{58}Co could be transported under colloidal form. Thus, if the previously described deposition model (which includes surface interactions) applied to the case of Reactor A is able to reproduce the preferential contamination in the crossover leg, the previous hypothesis could be confirmed. When using the new deposition model to simulated the contamination levels for Reactor A at cycle SGR + 1, the results presented in Fig. 12 are obtained. The new deposition model is able to reproduce the preferential contamination by a factor of 5.

The temperature of the medium considered has a direct effect on particle deposition as it affects the zeta potential value (Cherpin et al., 2022b) of both the particles and the deposit. In the case of Reactor A, the temperature of the hot leg and of the crossover leg are different (respectively around 323 °C and 287 °C respectively during the operating cycle) and so is the pH of the solution. This results in different values for the zeta potential of particles and of the deposition surface, directly influencing deposition.

As mentioned before, the zeta potential values used to compute the electrical double layer interaction and thus have access to the value of the potential barrier to overcome for deposition to happen at certain temperature-chemistry conditions come from an extrapolation of measured data between 20 °C and 240 °C. As temperatures in the primary system are comprised between 280 °C and 330 °C, the validity of the extrapolation will be verified with future zeta potential measurements.

It is important to mention that as the deposition model was modified,

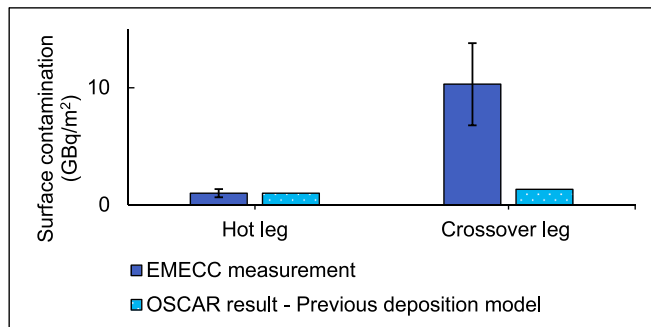


Fig. 10. Comparison between the normalized surface contamination in ^{58}Co measured with the EMECC device in the hot leg and cold leg at cycle SGR + 1 with the simulation obtained using the OSCAR code with the previous deposition model.

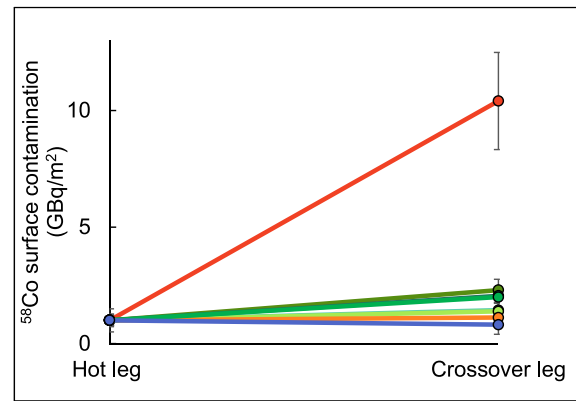


Fig. 11. Variation of the normalized surface contamination in ^{58}Co between the hot leg and the crossover leg for 8 different reactors one cycle after they underwent a SGR. The red line represents Reactor A.

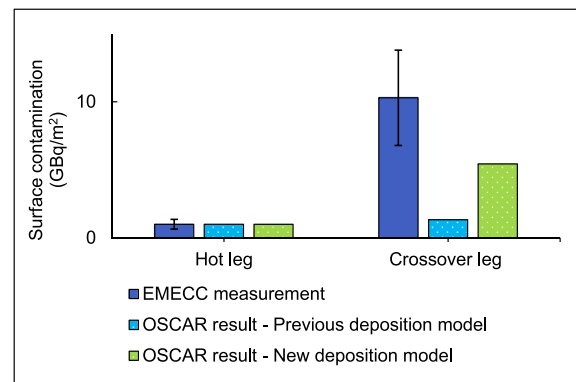


Fig. 12. Comparison between the surface contamination in ^{58}Co measured with the EMECC device in the hot leg and crossover leg at cycle SGR + 1 with the simulation obtained using the OSCAR code with the previous deposition model and the new deposition model.

calibration needs to be performed on other parameters (corrosion rates, erosion rate...) so that the simulation reproduces the EMECC measurement within acceptable boundaries.

It is the first time that the OSCAR code is able to reproduce preferential contamination in ^{58}Co in the cold legs. In fact, the model enables to link chemistry aspects (temperature, pH) of the primary coolant to particle deposition through the notion of zeta potential, which represents a novelty for the OSCAR code.

4. Conclusions

A new model aiming at predicting particle deposition has been developed for the OSCAR code. By accounting the various interactions at stake during particle deposition, the DLVO theory has been implemented to determine, if it exists, the potential barrier a particle has to overcome through its kinetic energy to deposit. Using the zeta potential values of particles previously measured up to 240 °C, the model was implemented in the OSCAR code. Using experiments performed on the CIRENE loop, the attachment probability profile was calibrated and the model validated, before being applied to the case of an operating 1300 MWe PWR. Using the new deposition model, the OSCAR code was able to reproduce for the first time, the preferential contamination in ^{58}Co of the crossover leg. This model represents a novelty as it draws a liaison between the chemistry of the solution and the physics of particles deposition.

CRedit authorship contribution statement

Chloé Cherpín: Conceptualization, Data curation, Formal analysis, Investigation, Methodology, Software, Visualization, Writing – original draft, Writing – review & editing. **Frédéric Dacquait:** Conceptualization, Methodology, Software, Supervision, Validation, Writing – original draft, Writing – review & editing.

Declaration of competing interest

The authors declare that they have no known competing financial interests or personal relationships that could have appeared to influence the work reported in this paper.

Data availability

The authors do not have permission to share data.

Acknowledgments

This work is performed thanks to the contribution of the CEA, EDF and Framatome.

References

- Anthoni, S., Ridoux, P., 1996. Origin of corrosion products in PWR primary circuits, in: Eurocor 96. Presented at the Session IX Nuclear Corrosion and Protection, ORI, Nice.
- Beal, S.K., 1970. Deposition of Particles in Turbulent Flow on Channel or Pipe Walls. *Nucl. Sci. Eng.* 40, 1–11.
- Beal, S.K., 1978. Correlations for the sticking probability and erosion of particles. *J. Aerosol Sci.* 9, 455–461.
- Beslu, P., Frejaville, G., Lalet, A., 1978. A computer code PACTOLE to predict activation and transport of corrosion products in PWR, in: Proceedings of the International Conference of Water Chemistry of Nuclear Reactors Systems 1. London, England, pp. 195–201.
- Beslu, P., 1990. Pactole: Prédiction du comportement et de l'activation des produits de corrosion dans le circuit primaire des réacteurs à eau légère (No. SCOS/LCC/90-096). Centre d'études nucléaires de Cadarache.
- Bridle, D.A., 1989. The nature and behavior of particulates in PWR primary coolant (No. NP-6640). EPRI.
- Carrette, F., 2002. Relâchement des produits de corrosion des tubes en alliage 690 de générateur de vapeur du circuit primaire des réacteurs à eau pressurisée (PhD thesis). Toulouse, INPT.
- Cherpín, C., 2022. Modeling the behavior of colloidal corrosion products in the primary circuit of Pressurized Water Reactors. University of New Brunswick. PhD thesis.
- Cherpín, C., Lister, D., Dacquait, F., Liu, L., 2021. Study of the Solid-State Synthesis of Nickel Ferrite (NiFe₂O₄) by X-ray Diffraction (XRD), Scanning Electron Microscopy (SEM) and Raman Spectroscopy. *Materials* 14, 2557. <https://doi.org/10.3390/ma14102557>.
- Cherpín, C., Lister, D., Dacquait, F., Liu, L., Weerakul, S., 2022a. Magnetite (Fe₃O₄) and nickel ferrite (NiFe₂O₄) zeta potential measurements at high temperature: Part I - Design, materials and preliminary characterization of an apparatus implementing the streaming potential method. *Be Publ.*
- Cherpín, C., Lister, D., Dacquait, F., Weerakul, S., Liu, L., 2022b. Magnetite (Fe₃O₄) and nickel ferrite (NiFe₂O₄) zeta potential measurements at high temperature: Part II - Results, study of the influence of temperature, boron concentration and lithium concentration on the zeta potential. *Colloids Surf. Physicochem. Eng. Asp.* 647, 129030 <https://doi.org/10.1016/j.colsurfa.2022.129030>.
- Dacquait, F., Andrieu, C., Berger, M., Bretelle, J.L., Rocher, A., 2002. Corrosion product transfer in french PWRs during shutdown, in: NPC 2002. Avignon, France.
- Dacquait, F., Andrieu, C., Guinard, L., Bretelle, J.L., Bardet, F., Brun, C., 2004. Status of primary system contamination in PWRs, in: International Conference on Chemistry in Water Reactors. San Francisco, USA.
- Dacquait, F., Estienne, C., Demarais, R., 2008. St-Laurent B2 - Cycle 21 Mesure de la contamination du circuit primaire lors de l'arrêt pour recharge - Impact du RGV (Technical report No. CEA/DEN/CAD/SMTM/LMTR/2006-031).
- Dacquait, F., Génin, J.B., Brissonneau, L., 2017. Modelling of the contamination transfer in nuclear reactors: The OSCAR code Applications to SFR and ITER, in: 1st IAEA Workshop on Challenges for Coolants in Fast Neutron Spectrum Systems. Vienna (Austria).
- Dacquait, F., Francescato, J., Tevissen, E., Génin, J.-B., You, D., Cherpín, C., Broutin, F., 2023. Simulation of Co-60 uptake on stainless steel and alloy 690 using the OSCAR v1.4 code integrating an advanced dissolution-precipitation model. *Nucl. Eng. Des.* 405, 112190 <https://doi.org/10.1016/j.nucengdes.2023.112190>.
- Derjaguin, B., 1993. A theory of interaction of particles in presence of electric double layers and the stability of lyophobic colloids and disperse systems. *Prog. Surf. Sci.* 43, 1–14.
- Derjaguin, B., Landau, L., 1941. Theory of the stability of strongly charged lyophobic sols and of the adhesion of strongly charged particles in solutions of electrolytes. *Acta Phys. Chim. URSS* 14, 633.
- Deshon, J., Hussey, D., Kendrick, B., McGurk, J., Secker, J., Short, M., 2011. Pressurized water reactor fuel crud and corrosion modeling. *J. Miner. Met. Mater. Soc.* 63, 64. <https://doi.org/10.1007/s11837-011-0141-z>.
- Epstein, N., 1988. Fouling science and technology. Melo LF, Bott TR, Bernardo CA editors, Dordrecht, The Netherlands.
- Epstein, Norman, 1988. Particulate Fouling of Heat Transfer Surfaces: Mechanisms and Models, in: Melo, L.F., Bott, T.R., Bernardo, C.A. (Eds.), *Fouling Science and Technology*. Springer Netherlands, Dordrecht, pp. 143–164. https://doi.org/10.1007/978-94-009-2813-8_10.
- Frattini, P., 1999. Characteristics of corrosion products in the loop and VVER plant primary systems (No. TP-114132). EPRI.
- Friedlander, S.K., Johnstone, H.F., 1957. Deposition of Suspended Particles from Turbulent Gas Streams. *Ind. Eng. Chem.* 49, 1151–1156. <https://doi.org/10.1021/ie50571a039>.
- Gardey, S., 1998. Etude de la corrosion généralisée des alliages 600, 690 et 800 en milieu primaire. Contribution à la compréhension des mécanismes. Université Pierre et Marie Curie, Paris VI, Paris VI. PhD thesis.
- Génin, J.B., Brissonneau, L., 2017. Validation against sodium loop experiments of corrosion product contamination code OSCAR-Na, in: International Conference on Fast Reactors and Related Fuel Cycles. Yekaterinburg, Russian Federation.
- Girard, M., Dacquait, F., 2012. Experimental study of particle deposition kinetics in the primary circuit of the cirene loop and comparison with Oscar v1.2 code simulations. Presented at the International Conference on Water Chemistry in Nuclear Reactor Systems, Paris, France.
- Girard, M., Mombellet, R., 2011. Compte Rendu de l'essai en boucle "CIRENE 2010" (No. DEN/CAD/DTN/SMTN/LMTR/2011/27/0).
- Laufer, J., 1954. The Structure of Turbulence in Fully Developed Pipe Flow (Report No. TR-1174). National Advisory Committee for Aeronautics.
- Lin, C.S., Moulton, R.W., Putnam, G.L., 1953. Mass Transfer between Solid Wall and Fluid Streams. Mechanism and Eddy Distribution Relationships in Turbulent Flow. *Ind. Eng. Chem.* 45, 636–640. <https://doi.org/10.1021/ie50519a048>.
- Lister, D.H., 2012. Understanding and mitigating corrosion in nuclear reactor systems, in: *Nuclear Corrosion Science and Engineering*. Elsevier, pp. 57–74. <https://doi.org/10.1533/9780857095343.1.57>.
- Marchetti-Sillans, L., 2007. Corrosion généralisée des alliages à base nickel en milieu aqueux à haute température : Apport à la compréhension des mécanismes (PhD thesis). Ecole Nationale Supérieure Des Mines De Saint-Etienne.
- Millett, P., 1999. PWR Primary Water Chemistry Guidelines (No. TR-105714-V2R4). EPRI, Palo Alto.
- Ponting, A., 1983. Intrinsic filtration and retarded deposition for the control of colloidal corrosion product deposition on PWR fuel. *Water Chem.* 43–51.
- Rafique, M., Mirza, N., Mirza, S., 2010. Review of computer codes for modeling corrosion product transport and activity build-up in light water reactors. *Nukleonika* 50, 265–269.
- Rodliffe, R.S., 1985. Modelling the behaviour of corrosion products in the primary heat transfer circuits of pressurised water reactors - A Review of Principles (No. TPRD/B/0648/N85). Berkeley Nuclear Laboratories.
- Rudolph, L., 2016. CFD calculation method for the assessment of the impact of film-forming amines on local deposition at the tube sheet of steam generators. Presented at the 20th International Conference on Water Chemistry in Nuclear Reactor Systems, Brighton, United Kingdom.
- Sehmel, G.A., 1971. Complexities of particle deposition and re-entrainment in turbulent pipe flow. *J. Aerosol Sci.* 2, 63–72. [https://doi.org/10.1016/0021-8502\(71\)90008-5](https://doi.org/10.1016/0021-8502(71)90008-5).
- Strasser, A.A., 1996. Primary water chemistry, fuel rod corrosion, and crud deposition in PWRs – a comparison of european and US plant performance (No. R-107255). EPRI.
- Urrutia, G.A., Passaggio, S.I., Maroto, A.J.G., Blesa, M.A., 1983. Model of the Deposition of Colloidal Crud Particles on the Fuel Elements of Nuclear Power Plants. *Nucl. Sci. Eng.* 84, 120–130.
- Van Oss, C.J., Giese, R.F., Costanzo, P.M., 1990. DLVO and Non-DLVO interactions in hectorite. *Clays Clay Miner.* 38, 151–159.
- Verwey, E., Overbeek, J., 1948. Theory of the stability of lyophobic colloids. *J. Phys. Colloid Chem.* 51, 631.
- Watkinson, A.P., 1968. Particulate fouling of sensible heat exchangers.
- Wen, T., 1998. Corrosion products characterization and radiation field buildup with Li/B modified chemical condition for Maanshan nuclear power plant, in: Proceedings of the 1998 JAIF International Conference on Water Chemistry in Nuclear Power Plants. Kashiwazaki, Niigata, Japan.